Dhaka Univ. J. Sci. 68(1): 19- 28, 2020 (January)

Effect of Heat Generation and Thermal Radiation on the Slip Flow of Time Dependent Elastico-viscous Maxwell Nanofluid Flow Over a Porous Stretching Inclined Surface

M. Abdus Samad[1*] and M. Enamul Karim[1,2]

[1]*Department of Applied Mathematics, University of Dhaka, Dhaka-1000, Bangladesh*
[2]*Department of Mathematics, Comilla University, Cumilla-3506, Bangladesh*

(Received: 30 April 2019; Accepted: 7 January 2020)

Abstract

The present paper deals with the numerical analysis of the combined effect of heat generation and thermal radiation on the flow of a time dependent elastico-viscous Maxwell nanofluid passing over a stretching porous inclined surface with slip boundary. Appropriate similarity transformations are used to decorate the governing equations into a set of ordinary non-linear differential equations. The coupled ordinary equations are solved numerically using the Nachtsheim-Swigert shooting method together with the Runge-Kutta iterative technique for various values of the flow control parameters. In addition, the built-in function bvp4c of MATLAB is used to enhance the consistency of numerical results. The numerical results, demonstrated graphically, are described from the physical point of view. Finally, the effects of relevant parameters on the local skin-friction coefficient, the local Nusselt number, and the local Sherwood number, which are of material concern, are demonstrated in tabular form.

Keywords: Deborah number, Maxwell fluid, Nanofluid, Radiation, Slip condition.

I. Introduction

The low thermal conductivity of traditional heat transfer fluids like water, engine oil, kerosene and ethylene glycol is a prime limitation in developing the performance of modern engineering equipments. Nanofluids are the new-generation heat transfer fluids which hold higher thermal conductivity at very low particle concentrations than the conventional fluids. They are engineered by the uniform dispersion and stable suspension of a small amount of nanometer-sized (1–100 nm in diameter) ultrafine metallic, nonmetallic, ceramic or oxide particles in ordinary heat transfer fluids. Choi and Eastman[1] first developed the thought of nanofluid following the idea of colloidal suspension in regular fluid. Wong and Leon[2] reported that recent researchers have identified that the substitution of the usual refrigerants for nanofluids can be advantageous in processes such as the development of heat transport efficiency in the nuclear space and engineering, the cooling of motors and microelectronics, chillers, domestic refrigerators / freezers. Due to the mounting demand for encompassing extraordinary characteristics of providing unique physical and chemical properties nanofluids are receiving significant interest of many scientists and researchers[3,4].

Mushtaq *et al.*[5] reported that the multiplicity practical purposes of non-Newtonian fluids are the main focus of the last decades on technology and industrial processes, for example in geophysics, petroleum, biomedical and chemistry. Mustafa and Mushtaq[6] explicated that the equations of momentum of these fluids are extremely nonlinear and the Navier-Stokes equations certainly are not sufficient to demonstrate the non-Newtonian fluid flow. Almost all rheological complex fluids for examples industrial and biological fluids such as polymer solutions, paints, pulps, fossil fuels, molten plastics, liquid foods, jams, and blood exhibit the non-linear bonding between stress and deformation rate[7,8]. The Maxwell fluid model enclosed with viscoelastic material is the simplest subclass of rate-type non-Newtonian fluids and capable of explaining the characteristics of relaxation time effects on fluid, sorted out by Gallegos and Martínez-Boza[9]. An innovative work done by Harris[10] portraying 2D flow of Maxwell fluids is promoting the researchers to explore the more potential. Following this route, Fetecau *et al.*[11] have recently explored the viscoelastic fluid flow by way of fractional Maxwell model subjected to time dependent shear stress. Sochi[12] condensed the Maxwell fluid model into the Navier-Stokes relation when the relaxation time effect is deficient.

Very recent, a number of researchers investigated a choice of parametric effects like thermal radiation, Joule heating and heat source on fluid flow passing above a stretching porous sheet[13-16]. Sparrow and Cess[17] explained Rosseland approximation to describe the radiation heat flux in the energy equation in their book.

The objective of this article is to analyze the combined effect of thermal radiation and heat source on unsteady two-dimensional laminar flow of elastico-viscous silver (*Ag*)-water nanofluid passing over the porous stretching surface with slip boundary applying the Maxwell rheological fluid model. The present Maxwell nanofluid model has been considered to study the time dependent stress relaxation of viscoelastic fluid hosting solid nanoparticles. In fact, the Maxwell non-Newtonian fluid with enhanced heat transfer offers an excellent opportunity to contribute to industrial and hemodynamic purposes.

II. Mathematical Formulation

The present model is made by considering a two-dimensional unsteady flow of an electrically conducting elastico-viscous non-Newtonian nanofluid in presence of

[*]Author for correspondence. e-mail: samad@du.ac.bd

magnetic field with the combined effect of radiation and heat generation passing a semi-infinite stretching porous surface with slip boundary inclined with an angle α to the vertical. When elastic stress is applied to a non-Newtonian fluid, the resulting strain is time dependent characterized by the relaxation time. The constitutive equation for a Maxwell fluid[8,18] is

$$\mathbf{T} = -p\mathbf{I} + \mathbf{S}, \tag{1}$$

where $\mathbf{T}$ is the Cauchy stress tensor and the extra stress tensor $\mathbf{S}$ satisfies

$$\mathbf{S} + k\left(\frac{d\mathbf{S}}{dt} - \mathbf{LS} - \mathbf{SL}^{\mathrm{tr}}\right) = \mu_0 \mathbf{A}_1 \tag{2}$$

in which μ_0 is the viscosity, $k > 0$ is the relaxation time and the Rivlin–Ericksen tensor $\mathbf{A}_1$ is defined through

$$\mathbf{A}_1 = \nabla\mathbf{V} + (\nabla\mathbf{V})^{\mathrm{tr}}. \tag{3}$$

The relaxation time for Maxwell fluid is considered by $k = k_0(1-\lambda t)$, where k_0 is the initial value at $t = 0$. Moreover, the nanofluid as a mixture of the water and Ag nanoparticles is discussed here. To explain the physical configuration, the Cartesian coordinate system is introduced such a way that $x-$axis is measured along the plate surface and $y-$axis is perpendicular to the plate. The plate surface is placed at the plane $y = 0$ shown in Fig. 1. The free fluid flow $U_\infty(x,t) = ax/(1-\lambda t)$ is assumed to be detained to $y > 0$ due to the buoyancy force and non-uniform magnetic field of strength $B = B_0/\sqrt{1-\lambda t}$ applied normal to the surface; B_0 is the initial strength of the magnetic field. It is important to note here that, the expressions for $U_\infty(x,t)$ and B are valid only for time $t < \lambda^{-1}$ unless $\lambda = 0$.

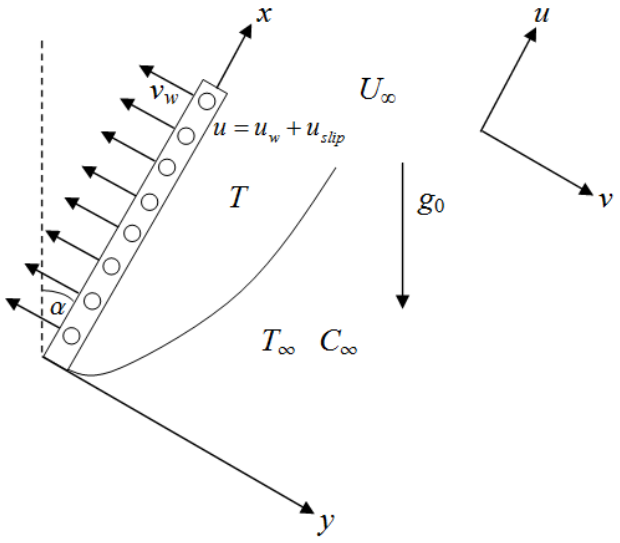

Fig. 1. Flow geometry of the model

Taking the above observations into account and using the Buongiorno nanofluid model incorporating the combined effect of thermophoresis and Brownian motion[19,20], the equations for mass, momentum, thermal energy, and nanoparticles concentration for a Maxwell fluid are[21]

$$\frac{\partial u}{\partial x} + \frac{\partial v}{\partial y} = 0 \tag{4}$$

$$\begin{aligned}\frac{\partial u}{\partial t} + u\frac{\partial u}{\partial x} + v\frac{\partial u}{\partial y} + k\left(u^2\frac{\partial^2 u}{\partial x^2} + v^2\frac{\partial^2 u}{\partial y^2} + 2uv\frac{\partial^2 u}{\partial x \partial y}\right) \\ = \nu_{nf}\frac{\partial^2 u}{\partial y^2} - \frac{\sigma_{nf}B^2 u}{\rho_{nf}} \\ + g_0\beta_T(T - T_\infty)\cos\alpha + g_0\,\beta_T^*(C - C_\infty)\cos\alpha\end{aligned} \tag{5}$$

$$\begin{aligned}\frac{\partial T}{\partial t} + u\frac{\partial T}{\partial x} + v\frac{\partial T}{\partial y} = \frac{\kappa_{nf}}{(\rho c_p)_{nf}}\frac{\partial^2 T}{\partial y^2} \\ + \tau_{nf}\left[D_B\frac{\partial T}{\partial y}\frac{\partial C}{\partial y} + \frac{D_T}{T_\infty}\left(\frac{\partial T}{\partial y}\right)^2\right] \\ + \frac{Q^*}{(\rho c_p)_{nf}}(T - T_\infty) - \frac{1}{(\rho c_p)_{nf}}\frac{\partial q_r}{\partial y}\end{aligned} \tag{6}$$

$$\frac{\partial C}{\partial t} + u\frac{\partial C}{\partial x} + v\frac{\partial C}{\partial y} = D_B\frac{\partial^2 C}{\partial y^2} + \frac{D_T}{T_\infty}\frac{\partial^2 T}{\partial y^2} \tag{7}$$

Considering the velocity slip proportional to the local shear stress, the governing equations are associated with the boundary conditions:

$$\left.\begin{aligned} &u = u_w(x,t) + u_{slip}(x,t),\ v = v_w, \\ &\quad T = T_w,\quad C = C_w \quad \text{at}\ \ y = 0 \\ &u = 0,\ T = T_\infty,\quad C = C_\infty \quad \text{as}\ \ y \to \infty \end{aligned}\right\} \tag{8}$$

where g_0 is the acceleration due to gravity, β_T is the volumetric coefficient of thermal expansion, β_T^* is due to concentration, D_B and D_T are the Brownian and thermophoresis diffusion respectively. $u_w(x,t) = bx/(1-\lambda t)$ is the stretching velocity, where the initial stretching rate b and the time scale λ are the positive constants having dimensions time^{-1}, and $b/(1-\lambda t)$ is the effective increasing stretching rate with time. $u_{slip}(x,t) = N\sqrt{1-\lambda t}\,\frac{\partial u}{\partial y}$ is the slip velocity, $T_w = T_\infty + ax/(1-\lambda t)^2$ and $C_w = C_\infty + ax/(1-\lambda t)^2$ are the temperature and concentration respectively assumed to vary both along the surface and with time, T_∞ and C_∞ are the temperature and concentration of free stream respectively. Relations among the physical properties of nanofluid[22,23] are given by

$$\rho_{nf} = (1-\varphi)\rho_f + \varphi\rho_s, \qquad \alpha_{nf} = \frac{\kappa_{nf}}{(\rho Cp)_{nf}}, \quad \mu_{nf} = \frac{\mu_f}{(1-\varphi)^{2.5}},$$
$$(\rho Cp)_{nf} = (1-\varphi)(\rho Cp)_f + \varphi(\rho Cp)_s,$$
$$\frac{\kappa_{nf}}{\kappa_f} = \frac{(\kappa_s + (n-1)\kappa_f) - (n-1)\varphi(\kappa_f - \kappa_s)}{(\kappa_s + (n-1)\kappa_f) + \varphi(\kappa_f - \kappa_s)}$$

Here the nanoparticles volume fraction is represented by φ. Also ρ, κ, α, C_p and σ are the density, thermal conductivity, thermal diffusivity, heat capacitance and electrical conductivity respectively. Here, suffices *f*, *s* and *nf* represent the base fluid, solid nanoparticles and nanofluid respectively. $n = \frac{3}{\Psi}$ is the nanoparticles shape factor for thermal conductivity and $\Psi = 1$ for spherical shape of nanoparticles is defined by Maxwell[22]. The thermo-physical properties of base fluid water and other different nanoparticles (*Ag*, *Cu*, Al_2O_3, and TiO_2) are given in the Table 1.

Table 1. Thermo-physical properties of water as the base fluid and different nanoparticles[6,23]

Materials	ρ	Cp	κ
Water	997.1	4179	0.613
Silver (Ag)	10500	235	429
Copper (Cu)	8933	386	401
Alumina (Al_2O_3)	3970	765	40
Tinanium Oxide (TiO_2)	4250	686.2	8.9538

To describe the transport mechanisms in nanofluids, it is significant to make the equations dimensionless using the similarity transformations. The main outcomes of making the equations dimensionless are (i) to understand the controlling flow parameters of the system (ii) to get rid of dimensional constraint. Form the above point of view, the governing equations can be reduced to dimensionless forms using the following similarity transformations[24].

$$\eta = y\sqrt{\frac{a}{\nu_f(1-\lambda t)}}, \qquad \psi = \sqrt{\frac{\nu_f a}{(1-\lambda t)}}\, x\, f(\eta)$$
$$T(x,t) = T_\infty + \frac{ax}{(1-\lambda t)^2}\theta(\eta), \; C(x,t) = C_\infty + \frac{ax}{(1-\lambda t)^2}F(\eta)$$

Using the above transformations, equation (4) is satisfied and the equations (5)–(7) are reduced to

$$\frac{\nu_{nf}}{\nu_f} f''' + \left(ff'' - f'^2 - A\left(\frac{\eta}{2}f'' + f'\right) - \beta\left(f^2 f''' - 2ff'f''\right)\right) - \frac{\sigma_{nf}\rho_f}{\sigma_f\rho_{nf}} M^2 f' + Gr_x \cos\alpha\,\theta + Gr_x^* \cos\alpha\, F = 0 \tag{9}$$

$$\frac{\kappa_{nf}}{\kappa_f}\frac{(\rho Cp)_f}{(\rho Cp)_{nf}}\frac{1}{Pn}\theta'' + \left(f\theta' - f'\theta - A\left(\frac{\eta}{2}\theta' + 2\theta\right)\right) + Nb\theta' F' + Nt\theta'^2 + \frac{(\rho Cp)_f}{(\rho Cp)_{nf}} Q\theta = 0 \tag{10}$$

$$F'' + Le\left(fF' - f'F - A\left(\frac{\eta}{2}F' + 2F\right)\right) + \frac{Nt}{Nb}\theta'' = 0 \tag{11}$$

Subjected to the dimensionless boundary conditions:

$$\left.\begin{array}{ll} f' = \gamma + \delta f'', \; f = fw, \; \theta = 1, \; F = 1 & \text{at } \eta = 0 \\ f' = 0, \qquad\qquad\qquad \theta = 0, \; F = 0 & \text{as } \eta \to \infty \end{array}\right\} \tag{12}$$

Here $\gamma = \frac{b}{a}$ is the stretching parameter; $\delta = N\sqrt{\frac{a}{\nu_f}}$ is the slip parameter; $A = \frac{\lambda}{a}$ is the unsteadiness parameter; $\beta = k_0 a$ is the Maxwell parameter; $M = \sqrt{\frac{\sigma B_0^{\,2}}{a\rho_f}}$ is the Magnetic field parameter; $Nb = \frac{\tau_{nf} D_B \Delta C_\infty}{\nu_f}$ is the Brownian motion parameter; $\Pr = \frac{\nu_f (\rho c_p)_f}{\kappa_f}$ is the Prandtl number; $Rn = \frac{\kappa_{nf}\kappa_1}{4\sigma_1 T_\infty^3}$ is the radiation parameter and $Pn = \frac{3Rn\Pr}{3Rn+4}$, $Q = \frac{Q_0}{a(\rho c_p)_f}$ is the heat source (Q>0)/ sink (Q<0) parameter $Nt = \frac{\tau_{nf} D_T \Delta T_\infty}{\nu_f T_\infty}$ is the thermophoresis parameter; $fw = -\sqrt{\frac{1-\lambda t}{\nu_f a}}v_0$ is the suction parameter; and $Le = \frac{\nu_f}{D_B}$ is the Lewis number.

The parameters of engineering interest for the present problem are the skin friction coefficient C_f, the Nusselt number *Nu* and Sherwood number *Sh* which indicate physically wall shear stress, rate of heat transfer, and mass transfer rate respectively.

$$C_f = \frac{1}{(1-\varphi)^{2.5}} f''(0), \; Nu = -\frac{\kappa_{nf}}{\kappa_f}\theta'(0), \; Sh = -F'(0) \tag{13}$$

III. Numerical Computation

Equations (9)–(11) combined with the boundary conditions (12) are solved numerically using the Runge-Kutta method with the Nachtsheim-Swigert shooting technique[25] for various values of the parameters nanoparticle volume fraction parameter (φ), Deborah number (β), magnetic field parameter (M), unsteadiness parameter (A), slip parameter (δ), stretching parameter (γ), suction parameter (f_w), Prandtl number $(\Pr)$, Radiation parameter (Rn), heat generation parameter (Q), thermophoretic parameter (Nt), Brownian motion parameter (Nb), Lewis number (Le). The step size is taken as $\eta = 0.01$ and the tolerance criteria are set to 10^{-6}. In order to strengthen the reliability of our results, a MATLAB boundary value problem solver called bvp4c is used. On the basis of a number of computational experiments, we are considering $[0,5]$ as the domain of the problem instead of $[0,\infty)$ because for $\eta > 5$ there is no significant variation in the results. The parametric values

$\varphi = 0.05,\ \beta = 0.5,\ M = 1,\ A = 0.5,\ \gamma = 0.1,\ \delta = 0.5,$ $f_w = 0.5,\ Rn = 1.0,\ Q = 0$. P r= 6 $Nt = 0$. $Nb = 0.4,$ and $Le = 10$ [21,24,26] are set for Ag-water nanofluid to verify the numerical results for both shooting method and MATLAB code showing in the Fig. 2.

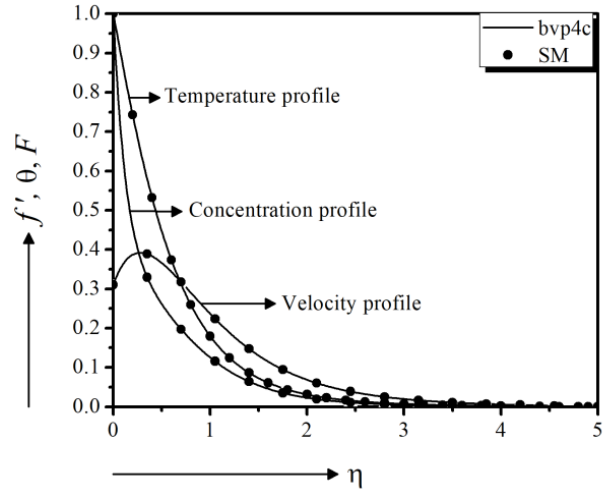

Fig. 2. Computational results from both Shooting Method (SM) and bvp4c function.

IV. Results and Discussion

Figure 2 is giving significant agreement to validate the numerical results obtained by shooting method and bvp4c function. But still for more contentment, it is necessary to certify our codes by comparing with some published works of similar nature. For this purpose, we have analyzed the numerical values of local skin friction coefficient $f''(0)$ for the models investigated by several researchers. A remarkable agreement of our results with those of models can be seen in Table 2.

Table 2. Comparison of $f''(0)$ for taking Pr = 0.71, *Nb*=0.1, *Nt* = 0.1, *Le* = 5, γ=1.

A	Madhu *et al.*[21]	Sharidan *et al.*[27]	Present work	
			bvp4c	SM
0.8	-1.261211	-1.261042	-1.261042	-1.261495
1.2	-1.377625	-1.377722	-1.377724	-1.377644

First, the nume rical calculation of the velocity, temperature, concentration, skin friction, heat and mass transfer profiles is performed for water-based nanofluids containing different solid nanoparticles (*Ag*, *Cu*, Al_2O_3, TiO_2) individually using a volume fraction of 5%, in Fig. 3–8. It is observed that Al_2O_3-water has higher velocity (in Fig. 3) as well as friction rate (in Fig. 6) and mass transfer rate (in Fig. 8). But *Ag*-water has higher temperature and concentration distribution (in Fig. 4–5). At the same phase, the heat transfer rate of TiO_2-water nanofluid is higher (in Fig. 7). *Ag*-water nanofluid is considered for the present model because of its valuable use in medical science[28,29].

When the elastic stress is applied to the non-Newtonian fluid, the time during which the fluid gains its stability is the relaxation time, which is greater for highly viscous fluids. The Deborah number β is a dimensionless variable that deals with fluid relaxation time to its characteristic time scale. Here β=0 gives the result for Newtonian viscous incompressible fluid. Fluids with small Deborah number exhibit liquid-like behavior whereas large Deborah number communicates with solid-like substances able to conduct and retain heat better. Therefore, it is observed physically that gradually increasing the Deborah number can increase the fluid viscosity, which enhances resistance to flow and, as a result, the hydrodynamic boundary layer thickness reduces for Maxwell fluid, as revealed in Fig. 9 for both steady (*A*=0) and unsteady (*A*=0.5) motion. This result is in agreement with the previous

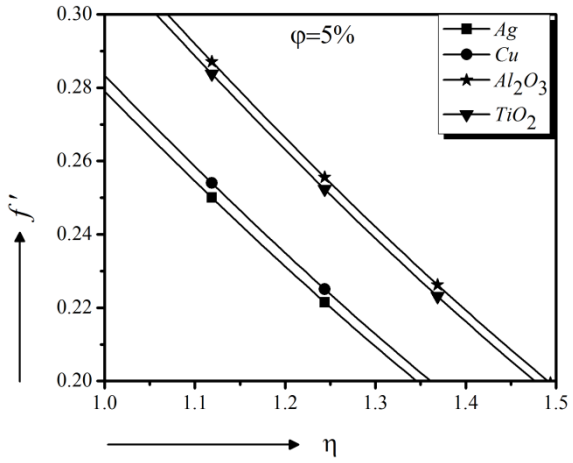

Fig. 3. Effect of nanoparticle volume fraction φ on velocity for different solid particles

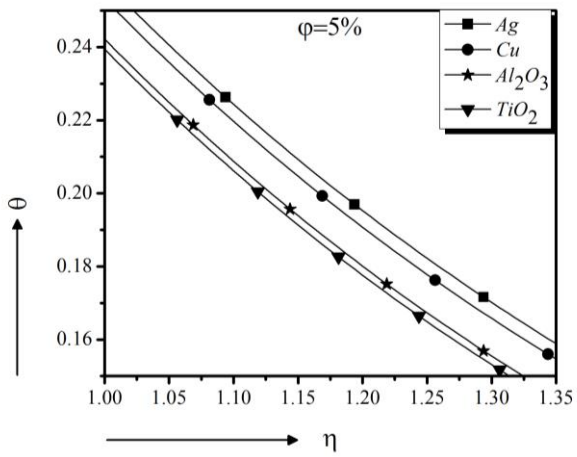

Fig. 4. Effect of nanoparticle volume fraction φ on temperature for different solid particles

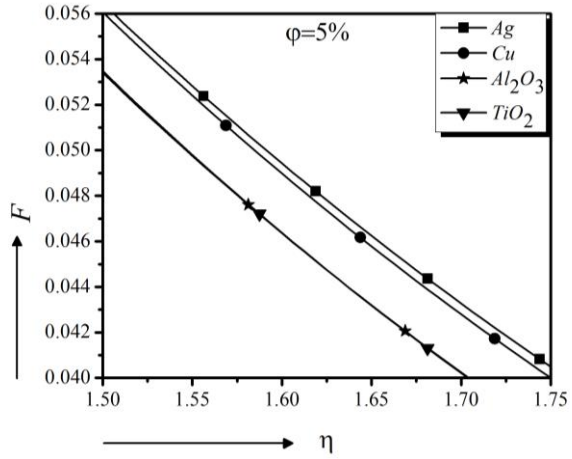

Fig. 5. Effect of nanoparticle volume fraction φ on concentration for different solid particles

study of Sadeghy *et al.*[30]. The positive effect of β is more prominent for steady motion. Figures 10–11 show very negligible effect of the Deborah number on the thermal boundary layer and solutal distribution respectively for both $A = 0$ and $A = 0.5$. These outcomes make a good agreement with Shateyi[15]. Such observations have a great contribution in the fiberglass industries[30].

From Fig. 12 it is seen that velocity decreases significantly with the increase of the radiation parameter *Rn* for cooling plate. It is also noticed that an increase in the magnetic parameter *M* reduces the velocity profiles. This is the result of the effect of the magnetic field imposed on an electrically conductive fluid, which generates a drag force called Lorentz force against the flow direction along the surface to slow down velocity. This is in accordance with the fact that the magnetic field is responsible for reducing the velocity of fluid flow. From Fig. 13 it is observed that the temperature decreases rapidly with the increase of *Rn* for both in the presence and absence of magnetic field because of emitting energy from thermal boundary layer. So, it is possible to control the flow characteristic and temperature using radiation parameter *Rn*. But in the same situation, concentration of fluid is getting higher due to the effect of radiation, in Fig. 14. These results are very similar to the work of Samad and Karim[31]. The analysis of such results could be beneficial to the polymer engineering [21].

For different values of heat generating parameter *Q*, the profile distributions are exposed for both porous (*fw*=0.5) and flat (*fw*=0) surface in Fig. 15–17. It is observed in Fig. 15 that due to the generation of heat, the buoyancy force increases, which accelerates the velocity in the boundary layer. Because of heat generation, the maximum velocity arises near the surface of the stretching plate for both situations *fw*=0 and *fw*=0.5. This is corroborated by Fig. 16 that the temperature do indeed rapid increase as higher *Q* affixes supplementary heat to the fluid. The hydrodynamic and thermal boundary layers thickness increase but the higher heat generation increase the molecular movement in fluid and hence reduce the concentration layer, in Fig. 17.

The effect of the surface inclination angle α on velocity is revealed in Fig. 18. From this figure it is depicted that that the velocity reduces with higher angle[31] α where the dashed line represents the horizontal surface for $\alpha = \pi / 2$. As angle increases, the buoyancy force reduces and hence the velocity decreases. Figure 19 shows that temperature rise rapidly with the higher α. Finally, it is seen in Fig. 20 that the angle of inclination shows very irrelevant effect on the concentration.

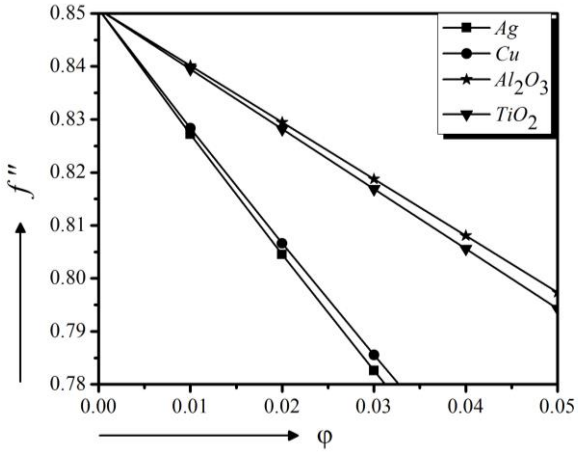

Fig. 6. Effect of nanoparticle volume fraction φ on velocity gradient for different solid particles

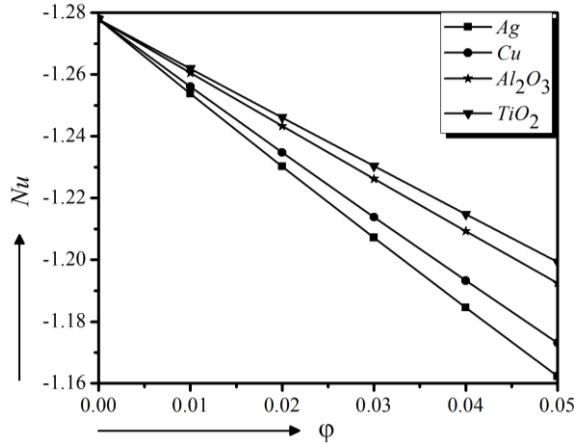

Fig. 7. Effect of nanoparticle volume fraction φ on temperature gradient for different solid particles

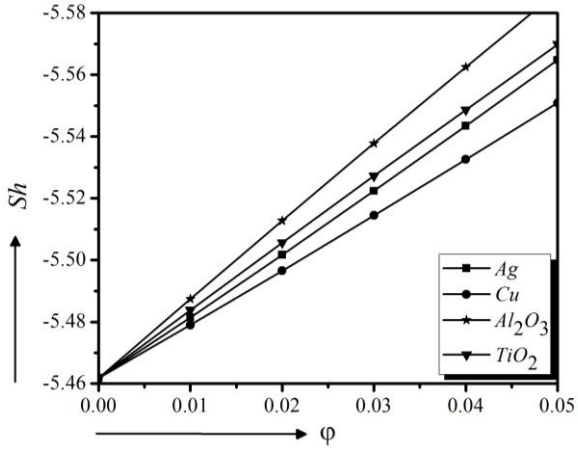

Fig. 8. Effect of nanoparticle volume fraction φ on concentration gradient for different solid particles

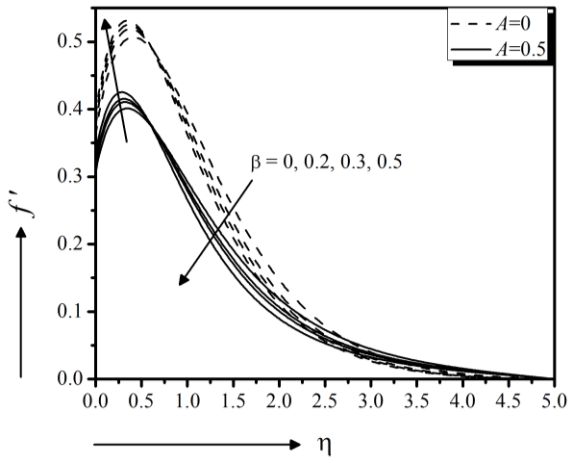

Fig. 9. Effect of Deborah number β on velocity for different solid particles

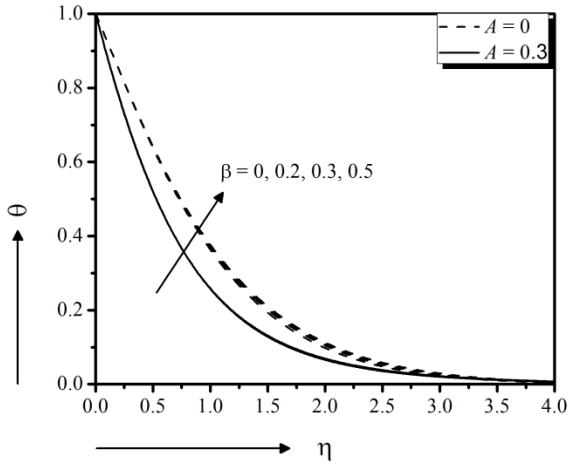

Fig. 10. Effect of Deborah number β on temperature for different solid particles

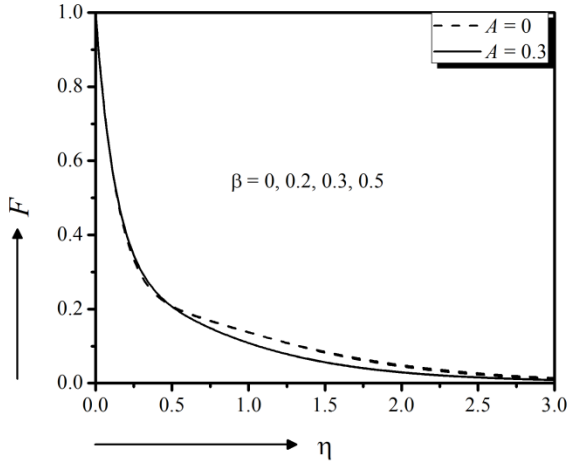

Fig. 11. Effect of Deborah number β on concentration for different solid particles

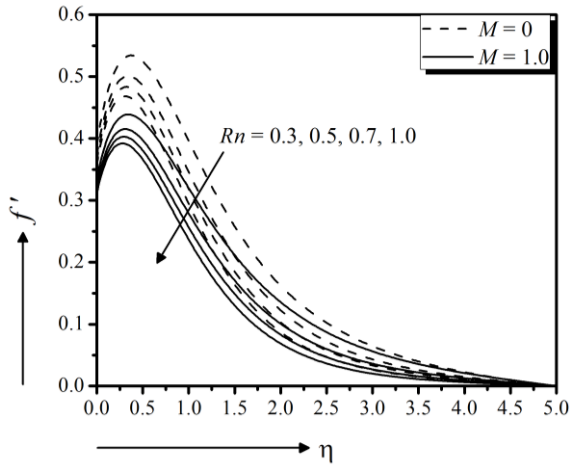

Fig. 12. Effect of radiation parameter *Rn* on velocity for different solid particles

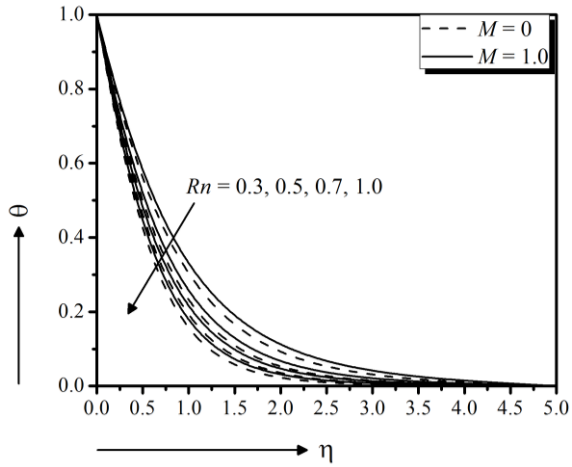

Fig. 13. Effect of radiation parameter *Rn* on temperature for different solid particles

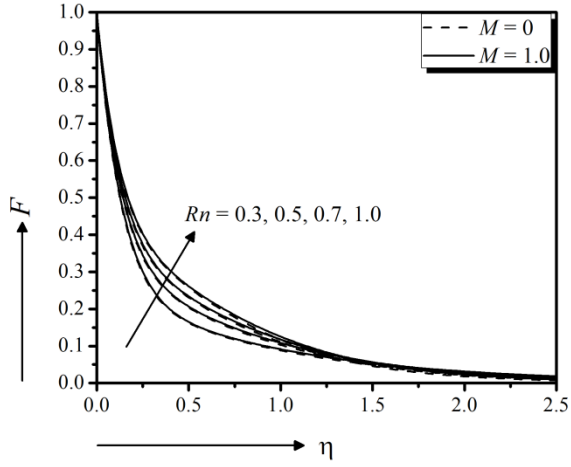

Fig. 14. Effect of radiation parameter *Rn* on concentration for different solid particles

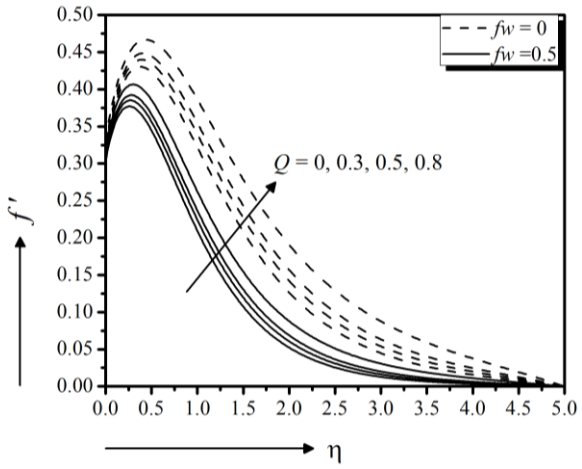

Fig. 15. Effect of heat generation parameter Q on velocity for different solid particles

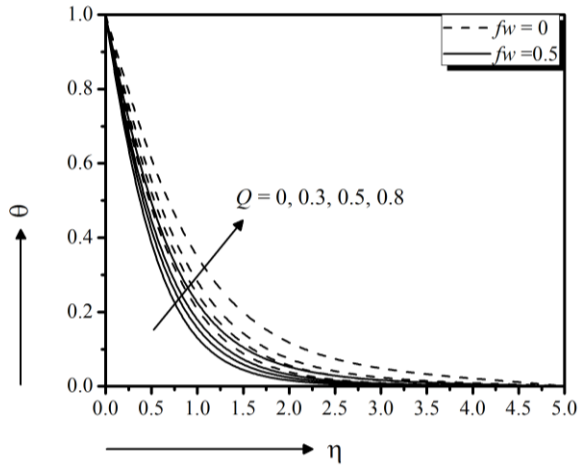

Fig. 16. Effect of heat generation parameter Q on temperature for different solid particles

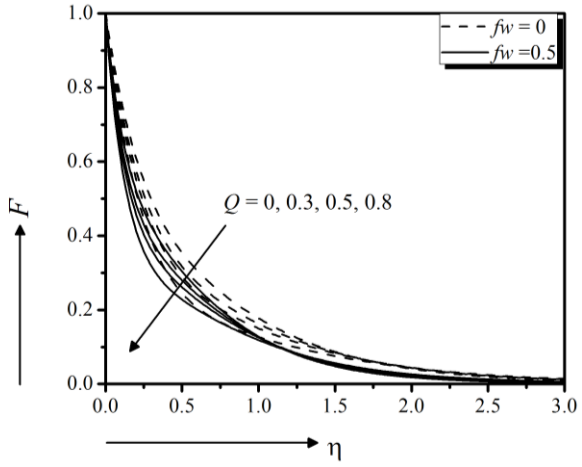

Fig. 17. Effect of heat generation parameter Q on concentration for different solid particles

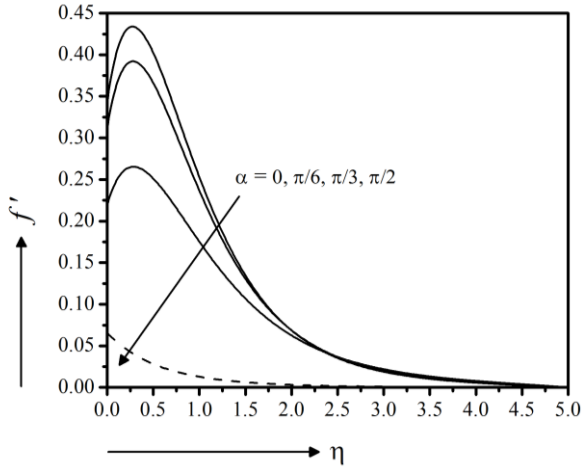

Fig. 18. Effect of inclination angle α on velocity for different solid particles

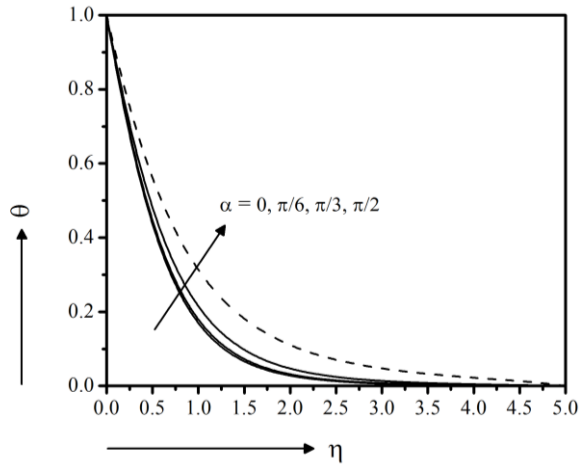

Fig. 19. Effect of inclination angle α on temperature for different solid particles

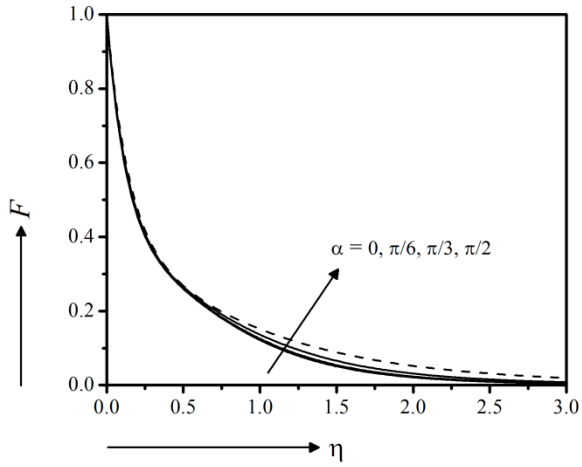

Fig. 20. Effect of inclination angle α on concentration for different solid particles

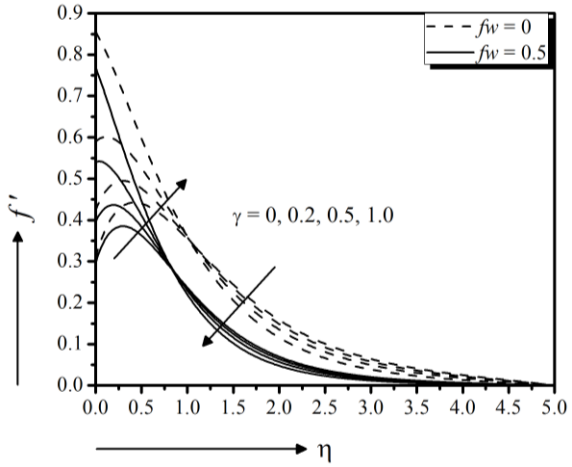

Fig. 21. Effect of stretching parameter γ on velocity for different solid particles

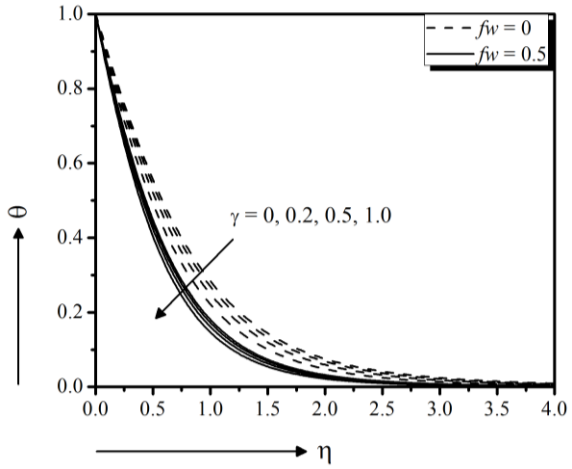

Fig. 22. Effect of stretching parameter γ on temperature for different solid particles

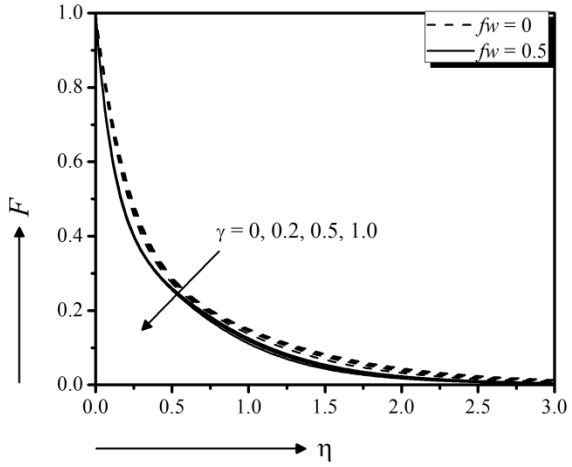

Fig. 23. Effect of stretching parameter γ on concentration for different solid particles

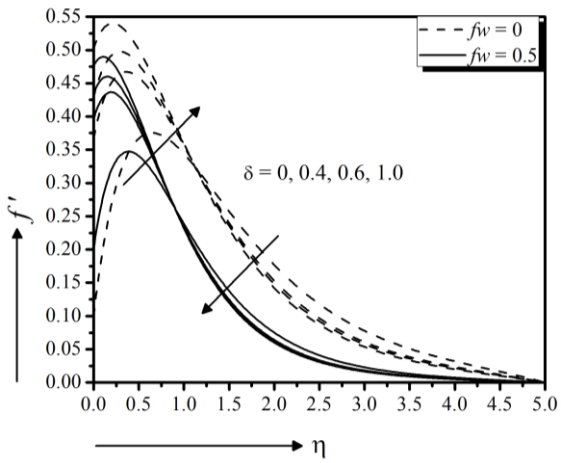

Fig. 24. Effect of slip parameter δ on velocity for different solid particles

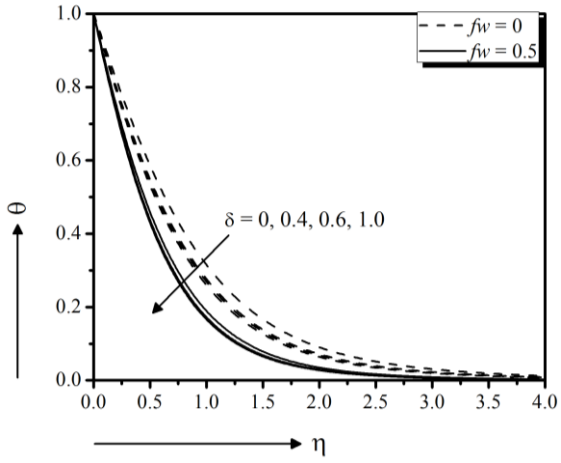

Fig. 25. Effect of slip parameter δ on temperature for different solid particles

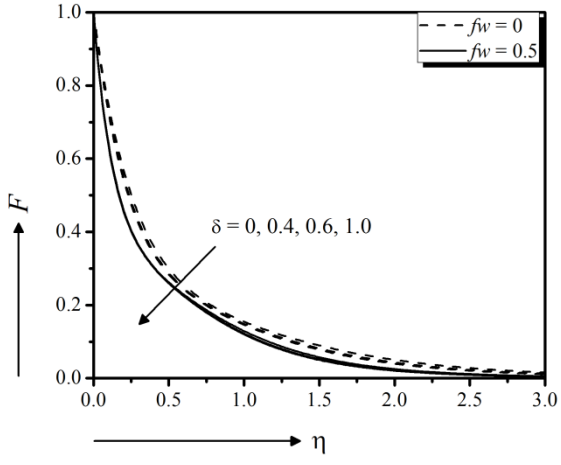

Fig. 26. Effect of slip parameter δ on concentration for different solid particles

Figure 21–23 depict the stretching parameter effect on momentum, energy and solutal distributions, respectively. From these figures it is observed that the stretching velocity enhances strength to the fluid velocity to increase the momentum distribution with the increase of stretching effect γ near the surface but away from the surface there occurs a cross flow and hence momentum distribution starts to decrease for both cases, in the presence and absence of suction parameter. The energy as well as solutal distribution is decreasing function of stretching parameter, showing good agreement with Nayak[32], for both suction and flat boundary surface. In addition, the imposed suction brings the distance of the fluid by improving the viscosity which in turn decelerates the fluid motion.

The results found from Fig. 24–26, similar to the findings carried out by Straughan and Harfash[33], are expressing the fact that the velocity increases near the surface but decrease away from the surface as the slip parameter δ increases both in the presence and absence of suction parameter. The energy as well as solutal distribution is falling function of δ. Slip factor is effective for the industrial purposes of reducing friction[34].

Finally, from the point of view of physical interest, the skin friction coefficient is useful to estimate the total frictional drag exerted on the surface. The Nusselt Number is used to characterize the heat flux from a heated solid surface to a fluid. The Sherwood number is used in mass-transfer operation. The Sherwood number is used in mass-transfer operation. Additionally, the effect of several variables on the skin fraction coefficient (f''), the local Nusselt number $(-\theta')$ and the local Sherwood number $(-F')$ are arranged in the Table 3.

Table 3. The effects of β and *Q* on the skin fraction coefficient, the local Nusselt number and the local Sherwood number.

β	Q	f''	$-\theta'$	$-F'$
0	0.5	0.69033	-1.15540	-5.55136
0.2	0.5	0.72341	-1.16007	-5.56030
0.3	0.5	0.74103	-1.16231	-5.56474
0.5	0	0.67741	-1.61303	-4.38525
0.5	0.3	0.69116	-1.46167	-4.83277
0.5	0.8	0.72619	-1.17011	-5.64329

V. Conclusions

The major outcomes drawn from the study of the present model can be summarized as follows:

- The heat transfer rate of TiO_2-water nanofluid is higher.
- The friction rate is lower for the increasing unsteadiness parameter and the mass transfer rates are much higher.
- The hydrodynamic boundary layer thickness reduces for the Maxwell fluid.
- Stretching and slip parameters can rule the model significantly.
- The magnetic field and the thermal radiation are liable for reducing the velocity of fluid flow.

In conclusion of the current study, it can be argued that the Maxwell parameter's velocity control phenomena and enhanced heat transfer in the liquid provide a great opportunity to develop cooling performance of mechanical system like bearings and automotive pistons with less friction.

References

1. Choi, S.U.S. and J. Estman, 1995. Enhancing thermal conductivity of fluids with nanoparticles. *ASME-Publications-Fed.* ***231***, 99-106.
2. Wong, K.V. and O. De Leon, 2010. Applications of nanofluids: current and future. *Advances in Mech. eng.* ***2***, 519659.
3. Buongiorno, J., L.-W. Hu, S.J. Kim, R. Hannink, B. Truong, and E. Forrest, 2008. Nanofluids for enhanced economics and safety of nuclear reactors: an evaluation of the potential features, issues, and research gaps. *Nuclear Technology.* ***162***(1), 80-91.
4. Emerich, D.F. and C. G. Thanos, 2006. The pinpoint promise of nanoparticle-based drug delivery and molecular diagnosis. *Biomol. Eng.* ***23***(4), 171-184.
5. Mushtaq, A., S. Abbasbandy, M. Mustafa, T. Hayat, and A. Alsaedi, 2016. Numerical solution for Sakiadis flow of upper-convected Maxwell fluid using Cattaneo-Christov heat flux model. *AIP Advances.* ***6***(1), 015208.
6. Mustafa, M. and A. Mushtaq, 2015. Model for natural convective flow of viscoelastic nanofluid past an isothermal vertical plate. *The European Phys. J. Plus.* ***130***(9), 178.
7. Bandelli, R., 1995. Unsteady unidirectional flows of second grade fluids in domains with heated boundaries. *Int. J. Non-linear Mech.* ***30***(3), 263-269.
8. Fetecau, C. and C. Fetecau, 2003. A new exact solution for the flow of Maxwell fluid past an infinite plate. *Int. J. Non-linear Mech.* ***38***(3), 423-427.
9. Gallegos, C. and F. Martínez-Boza, 2010. Linear viscoelasticity. *Rheology: encyclopaedia of life support systems (EOLSS), UNESCO. Eolss, Oxford.* 120-143.
10. Harris, J., 1977. *Rheology and non-Newtonian flow*. Longman Publishing Group, New York, 28-33.
11. Fetecau, C., A. Mahmood, and M. Jamil, 2010. Exact solutions for the flow of a viscoelastic fluid induced by a circular cylinder subject to a time dependent shear stress. *Communic. in Nonlinear Sci. Numeric. Sim.* ***15***(12), 3931-3938.
12. Sochi, T., 2010. Flow of non-newtonian fluids in porous media. *J. Polymer Sci. Part B: Polymer Physics.* ***48***(23), 2437-2767.

13. Nield, D.A. and A. Bejan, 2006. *Convection in porous media*. Vol. 3. Springer, New York.

14. Karim, M.E., M. Samad, and M.A. Sattar, 2011. Steady MHD Free Convection Flow with Thermal Radiation Past a Vertical Porous Plate Immersed in a Porous Medium. *Res. J. Math. Stat.* ***3***(4), 141-147.

15. Shateyi, S., 2013. A new numerical approach to MHD flow of a Maxwell fluid past a vertical stretching sheet in the presence of thermophoresis and chemical reaction. *Bd. Value Prob.* ***2013***(1), 196

16. Soundalgekar, V., M. Patil, and H. Takhar, 1981. MHD flow past a vertical oscillating plate. *Nuclear Eng. Design.* ***64***(1), 43-48.

17. Sparrow, E. and R. Cess, 1978. *Radiation heat transfer. Series in Thermal and Fluids Eng*. McGraw-Hill, New York.

18. Oldroyd, J., 1950. On the formulation of rheological equations of state. *Proc. R. Soc. Lond. A.* ***200***(1063), 523-541.

19. Buongiorno, J., 2006. Convective transport in nanofluids. *J. Heat Trans.* ***128***(3), 240-250.

20. Kuznetsov, A. and D. Nield, 2010. Natural convective boundary-layer flow of a nanofluid past a vertical plate. *Int. J. Thermal Sci.* ***49***(2), 243-247.

21. Madhu, M., N. Kishan, and A.J. Chamkha, 2017. Unsteady flow of a Maxwell nanofluid over a stretching surface in the presence of magnetohydrodynamic and thermal radiation effects. *Propulsion and Power Research.* ***6***(1), 31-40.

22. Maxwell, J.C., 1881. *A treatise on electricity and magnetism*. Vol. 1. Clarendon press, Oxford.

23. Uddin, M., K. S. Al Kalbani, M. Rahman, M. Alam, N. Al-Salti, and I. Eltayeb, 2016. Fundamentals of nanofluids: evolution, applications and new theory. *Int. J. Biomath. Systems Biology*. ***2***(1), 1-32.

24. Sithole, H.M., S. Mondal, P. Sibanda, and S.S. Motsa, 2017. An unsteady MHD Maxwell nanofluid flow with convective boundary conditions using spectral local linearization method. *Open Physics.* ***15***(1), 637-646.

25. Nachtsheim, P.R. and P. Swigert, 1965. Statisfaction of asymptotic boundary conditions in numerical solution of systems of nonlinear equations of boundary-layer type. NASA Technical note D-3004, National Aeronautics and Space Administration, Washington.

26. Hayat, T., M. Waqas, M.I. Khan, and A. Alsaedi, 2017. Impacts of constructive and destructive chemical reactions in magnetohydrodynamic (MHD) flow of Jeffrey liquid due to nonlinear radially stretched surface. *J. Mole. Liquids.* ***225***, 302-310.

27. Sridhara, V. and L. N. Satapathy, 2011. Al2O3-based nanofluids: a review. *Nanoscale Res. Let.* ***6***(1), 456.

28. Niu, Z. and Y. Li, 2013. Removal and utilization of capping agents in nanocatalysis. *Chem. Materials.* ***26***(1), 72-83.

29. Kumar, H., N. Venkatesh, H. Bhowmik, and A. Kuila, 2018. Metallic nanoparticles: a review. *Biomedical J. Scient. Technic. Res.* ***4***(2), 1-11.

30. Sadeghy, K., A.-H. Najafi, and M. Saffaripour, 2005. Sakiadis flow of an upper-convected Maxwell fluid. *Int. J. Non-Linear Mech.* ***40***(9), 1220-1228.

31. Samad, M.A. and M.E. Karim, 2009. Thermal radiation interaction with unsteady MHD flow past a vertical flat plate with time dependent suction. *Dhaka Uni. J. Sci.* ***57***(1), 113-118.

32. Nayak, M., 2016. Chemical reaction effect on MHD viscoelastic fluid over a stretching sheet through porous medium. *Meccanica.* ***51***(8), 1699-1711.

33. Straughan, B. and A. Harfash, 2013. Instability in Poiseuille flow in a porous medium with slip boundary conditions. *Microfluidics and nanofluidics.* ***15***(1), 109-115.

34. Mohyud-Din, S.T., U. Khan, N. Ahmed, and W. Sikander, 2015. A study of velocity and temperature slip effects on flow of water based nanofluids in converging and diverging channels. *Intl. J. App. Comp. Math.* ***1***(4), 569-587.